

Thin-Film Lithium Niobate Acoustic Resonator with High Q of 237 and k^2 of 5.1% at 50.74 GHz

Jack Kramer[†], Vakhtang Chulukhadze[†], Kenny Huynh[‡], Omar Barrera[†], Michael Liao[‡], Sinwoo Cho[†], Lezli Matto[‡], Mark S. Goorsky[†] and Ruochen Lu[†]

[†]Department of Electrical and Computer Engineering, The University of Texas at Austin, Austin, US

[‡]Department of Electrical Engineering, University of California Los Angeles, Los Angeles, US

kramerj99@utexas.edu

Summary— This work reports a 50.74 GHz lithium niobate (LiNbO_3) acoustic resonator with a high quality factor (Q) of 237 and an electromechanical coupling (k^2) of 5.17% resulting in a figure of merit (FoM, $Q \cdot k^2$) of 12.2. The LiNbO_3 resonator employs a novel bilayer periodically poled piezoelectric film (P3F) 128° Y-cut LiNbO_3 on amorphous silicon (a-Si) on sapphire stack to achieve low losses and high coupling at millimeter wave (mm-wave). The device also shows a Q of 159, k^2 of 65.06%, and FoM of 103.4 for the 16.99 GHz tone. This result shows promising prospects of P3F LiNbO_3 towards mm-wave front-end filters.

Keywords— acoustic resonator, lithium niobate, mm-wave, thin film devices, periodically poled piezoelectric film

I. INTRODUCTION

Mobile communication systems rely heavily on acoustic devices for sub-6 GHz front-end filtering and signal processing [1]. This success is largely due to the intrinsic benefits that acoustic devices offer over electromagnetic alternatives, specifically significantly reduced size and loss [2], [3]. Achieving high-performance acoustic resonators at millimeter wave (mm-wave) would allow for the deployment of compact filters for emerging applications [4]. However, scaling acoustic devices to higher frequencies has posed a significant challenge, with a large performance degradation occurring above 6 GHz (survey in Fig. 1). In order to synthesize filters, higher quality factors (Q) and electromechanical coupling (k^2) are desired to increase the figure of merit (FoM, $Q \cdot k^2$) of resonators at mm-wave. Promising material candidates for accomplishing this include thin film lithium niobate (LiNbO_3) [5], [6], lithium tantalate (LiTaO_3) [7], aluminum nitride (AlN) [8] and scandium aluminum nitride (ScAlN) [9]. While these material platforms offer intrinsically high k^2 and Q , achieving high-performance devices at mm-wave still poses a significant challenge.

Previously demonstrated scaling of acoustic device topologies was typically accomplished through direct reduction of the critical device dimension. In the cases of surface acoustic wave (SAW) or bulk acoustic wave (BAW) devices, this involves scaling the interdigitated transducer (IDT) pitch [10] or film thicknesses [11], respectively. This method poses significant challenges, as reduced lateral dimensions introduce fabrication difficulties as resolving ultra-fine features begins to pose a significant challenge. Similarly, ultra-thin films suffer from having a decreased volume relative to surface area scaled

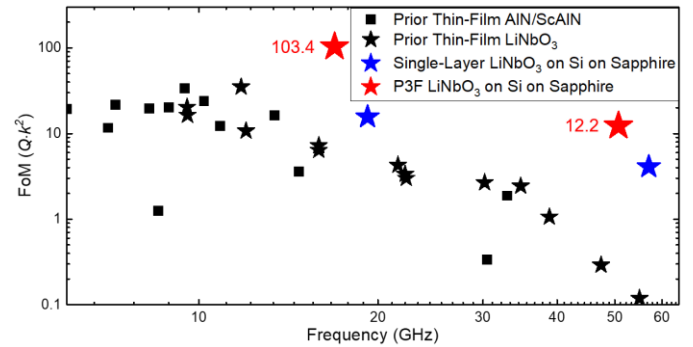


Fig. 1. Survey of state-of-the-art [18]–[20] acoustic resonator figure of merit (FoM) from 6 GHz to 60 GHz, with this work (red, bilayer P3F) and recent success (blue, single layer) using LiNbO_3 on Si on Sapphire highlighted.

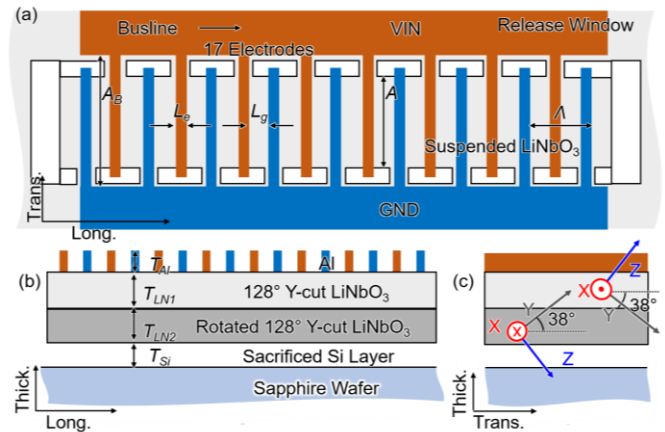


Fig. 2. (a) Top (b) cross-sectional, and (c) side schematic representations of the proposed P3F acoustic resonator design utilizing a bilayer P3F 128° Y-cut LiNbO_3 on a-Si on sapphire film-stack.

loss mechanisms, resulting in lower device Q . Thus, a device topology that allows for larger lateral feature sizes and retains thicker film thickness is highly desired.

One method by which scaling can be accomplished is to use higher-order antisymmetric Lamb modes in suspended thin-film LiNbO_3 [12]–[14]. This platform offers the benefit of having a very high intrinsic k^2 for a 128° Y-cut LiNbO_3 , which allows for the deployment of very wideband devices. While directly frequency scaling this device requires the thinning of the film, similar to in a film bulk acoustic resonator, one can

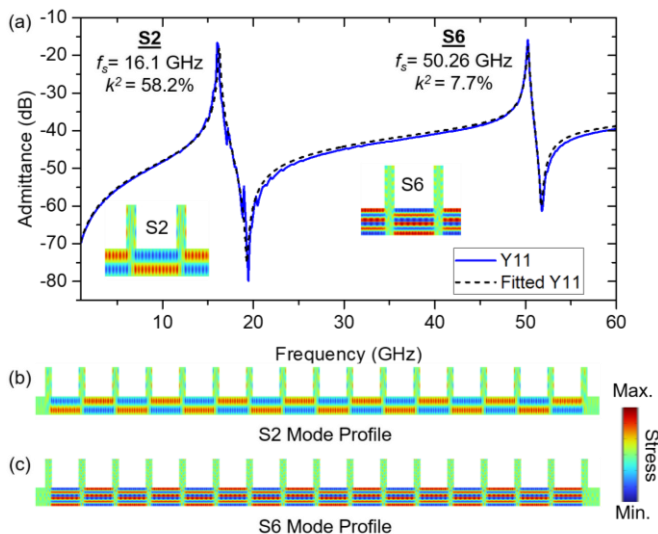


Fig. 3. (a) Simulated resonator admittance curves for the proposed film-stack with S2 and S6 tones at 16.1 GHz and 50.26 GHz respectively. (b), (c) Simulated mode stress profiles for the S2 and S6 tones, showing well confined acoustic modes within the film.

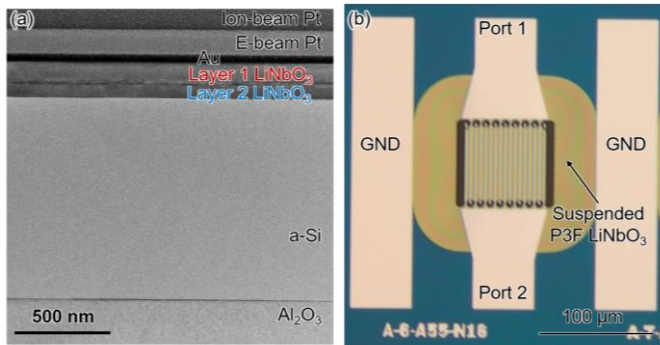


Fig. 4. (a) Transmission electron microscope (TEM) of the cross section of the film-stack. (b) Optical image of the acoustic resonator structure.

avoid this by using higher order antisymmetric modes. As an example, instead of operating in the first-order antisymmetric (A1), half-wavelength case, one can use the third-order antisymmetric (A3) mode. However, this comes with the trade off of a reduction in k^2 due to a cancellation in the electric field associated with an alternating displacement pattern [15]. To help mitigate this reduction in the coupling, a periodically poled piezoelectric film (P3F) stack can be employed. This topology allows for the symmetry of the device to be changed as to support the use of higher order modes. In the case of a bilayer P3F stack, the fundamental supported mode becomes the second-order symmetric (S2) mode. Since this consists of two A1 modes supported in each layer individually, the resultant S2 mode k^2 is the same as the A1 mode in a single-layer film. Thus, the P3F platform enables higher order modes while maintaining high coupling, a thicker total film stack, and large lateral feature sizes. Devices based on alternating orientation layers have been previously demonstrated with strong performance [16], [17], but the benefits have yet to be demonstrated at higher frequencies.

By employing the use of a novel film stack and the use of higher order second and sixth symmetric (S2 and S6, respectively) bulk acoustic tones in bilayer piezoelectric film (P3F) film stack, we are able to demonstrate record-breaking FoM performance at mm-wave.

II. DESIGN & SIMULATION

The proposed design is shown schematically in Fig. 2 (a)-(c). The design centers around a bilayer periodically poled P3F film stack with two bonded 128° Y-cut films. The two films are rotated 180° degrees relative to each other about the axis defined by the intersection of the YZ-plane and the 128° Y-cut plane. These layers sit upon a sacrificial layer of $1 \mu\text{m}$ of amorphous silicon (a-Si) on a $500 \mu\text{m}$ sapphire wafer. This platform is an iteration on a single layer LiNbO_3 platform, highlighted in blue in Fig. 1, which demonstrates the promise of the substrate and intermediate layer selection. The acoustic transducer consists of an interdigitated transducer (IDT) with 17 electrodes, with an electrode width (L_e) of 800 nm , an electrode gap (L_g) of $3.2 \mu\text{m}$, and a wavelength (λ) of $8 \mu\text{m}$. The aperture (A) of the device is $59 \mu\text{m}$, and 350 nm thick aluminum electrodes are selected. Etch windows $4 \mu\text{m}$ in height are positioned between the electrodes with a $1 \mu\text{m}$ gap between the edge of the electrode and the etch window. Etch windows $5 \mu\text{m}$ wide define the edge of the device, and the distance between the buslines (A_d) of the device is $71 \mu\text{m}$. The device is configured for a two-port measurement using $100 \mu\text{m}$ pitch GSG RF probes, with two $50 \mu\text{m}$ wide ground planes on the side of the device.

The proposed design was simulated using COMSOL finite element analysis (FEA) using an assumed LiNbO_3 thickness of 110 nm and Q of 200 for both layers. The admittance of the simulated device is shown in Fig. 3 (a), which showed an S2 tone at 16.1 GHz with a k^2 of 58.2% and an S6 tone at 50.26 GHz with a k^2 of 7.7% . The simulated mode profile for the S2 and S6 tones are well defined and well-constrained between the electrodes, as shown by the stress profile in Fig. 3 (b) and (c). Device parameters were optimized for the S6 tone, resulting in degraded S2 performance. However, the device still shows large k^2 at both tones.

III. FABRICATION AND RESULTS

The film stack was provided by NGK Insulators Ltd. and a film stack characterization was performed on a wafer edge piece prior to fabrication. A transmission electron microscope (TEM) cross-sectional image of the stack is shown in Fig. 4 (a). The TEM shows variation in the film thicknesses between the two LiNbO_3 layers, which is expected to contribute to spurious mode responses away from the two primary design resonances shown in the simulation. Using the TEM, the first layer thickness is measured to be 105 nm and the second layer to be 80 nm . However, due to the thickness variation across the wafer, the actual layer thickness is expected to be slightly different for the portion of the wafer used for the fabrication.

The fabricated resonator is shown in Fig. 4 (b). First, the two layers of LiNbO_3 are etched via photolithographic patterning and ion milling. Then, the 350 nm thick aluminum (Al) electrode and busline features are patterned using e-beam lithography and deposition. Finally, the LiNbO_3 is released

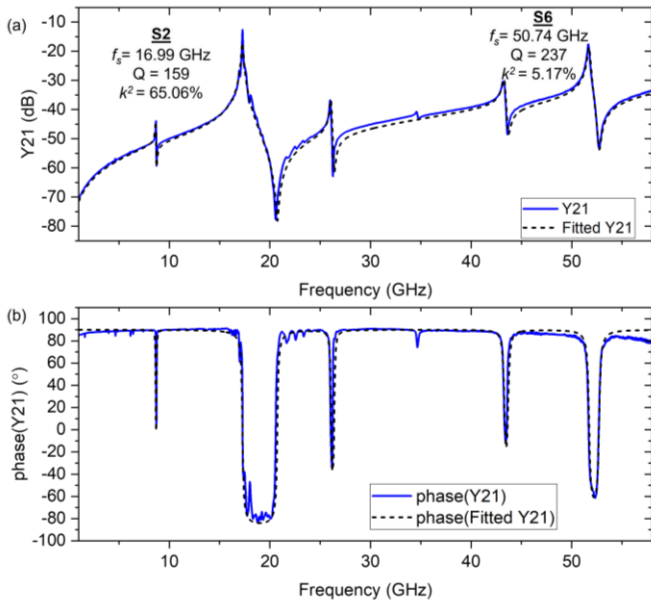


Fig. 5. (a) Measured admittance parameters and (b) phase of the fabricated device.

from the substrate with a xenon difluoride (XeF_2) based isotropic etch. This allows for mechanical isolation of the resonator from the substrate, greatly reducing mechanical losses.

The measured device admittance and phase curves are shown in Fig. 5 (a) and (b). The data was fitted with the use of a five motional branch modified Butterworth Van-Dyke model, which allowed for the fitting of the two primary S2 and S6 tones as well as three main spurious modes. The measured device shows state-of-the-art performance, with a 3 dB Q of 159 and k^2 of 65.06% for the 16.99 GHz S2 tones and a Q of 237 and k^2 of 5.17% for the 50.74 GHz S6 tone. The resultant FoM for the S2 and S6 tones are 103.4 and 12.2 respectively. The data shown and performance metrics both use raw data without any de-embedding. Comparison to SoA is plotted in Fig. 1, surpassing prior works at corresponding frequencies.

IV. CONCLUSION

This work presents a SoA 50.74 GHz LiNbO_3 acoustic resonator with a high 3 dB Q of 237 and k^2 of 5.17% for the targeted S6 mode. The associated S2 mode also significantly improves over state-of-the-art works, with a Q of 159 and k^2 of 65.06%. The record-breaking performance is enabled using a bilayer P3F stack utilizing a sacrificial amorphous Si layer on a sapphire substrate. This work demonstrates the possibility of achieving high FoM resonators at mm-wave, enabling the future synthesization of compact mm-wave filters.

ACKNOWLEDGMENT

The authors thank the DARPA COFFEE program for funding support and Dr. Ben Griffin for helpful discussions.

REFERENCES

[1] R. Ruby, "A Snapshot in Time: The Future in Filters for Cell Phones," *IEEE Microw Mag*, vol. 16, no. 7, pp. 46–59, 2015, doi: 10.1109/MMM.2015.2429513.

[2] S. Gong, R. Lu, Y. Yang, L. Gao, and A. E. Hassanien, "Microwave Acoustic Devices: Recent Advances and Outlook," *IEEE Journal of Microwaves*, vol. 1, no. 2, pp. 601–609, 2021, doi: 10.1109/JMW.2021.3064825.

[3] R. Lu and S. Gong, "RF acoustic microsystems based on suspended lithium niobate thin films: advances and outlook," *Journal of Micromechanics and Microengineering*, vol. 31, no. 11, p. 114001, Sep. 2021, doi: 10.1088/1361-6439/ac288f.

[4] A. Hagelauer et al., "From Microwave Acoustic Filters to Millimeter-Wave Operation and New Applications," *IEEE Journal of Microwaves*, vol. 3, no. 1, pp. 484–508, 2023, doi: 10.1109/JMW.2022.3226415.

[5] R. H. Olsson et al., "A high electromechanical coupling coefficient SH0 Lamb wave lithium niobate micromechanical resonator and a method for fabrication," *Sens Actuators A Phys*, vol. 209, pp. 183–190, 2014, doi: <https://doi.org/10.1016/j.sna.2014.01.033>.

[6] T. Kimura, M. Omura, Y. Kishimoto, and K. Hashimoto, "Comparative Study of Acoustic Wave Devices Using Thin Piezoelectric Plates in the 3–5-GHz Range," *IEEE Trans Microw Theory Tech*, vol. 67, no. 3, pp. 915–921, 2019, doi: 10.1109/TMTT.2018.2890661.

[7] L. Zhang et al., "High-Performance Acoustic Wave Devices on $\text{LiTaO}_3/\text{SiC}$ Hetero-Substrates," *IEEE Trans Microw Theory Tech*, pp. 1–11, 2023, doi: 10.1109/TMTT.2023.3267556.

[8] G. Piazza, V. Felmetzger, P. Muralt, R. H. Olsson III, and R. Ruby, "Piezoelectric aluminum nitride thin films for microelectromechanical systems," *MRS Bull*, vol. 37, no. 11, pp. 1051–1061, 2012, doi: DOI: 10.1557/mrs.2012.268.

[9] R. Vetry, A. S. Kochhar, and J. B. Shealy, "XBAW, An Enabling Technology for Next Generation Resonators and Filter Solutions for 5G and Wi-Fi 6/6E/7 applications (Invited)," in *2022 International Electron Devices Meeting (IEDM)*, 2022, pp. 16.1.1-16.1.4. doi: 10.1109/IEDM45625.2022.10019537.

[10] L. Colombo, A. Kochhar, C. Xu, G. Piazza, S. Mishin, and Y. Oshmyansky, "Investigation of 20% scandium-doped aluminum nitride films for MEMS laterally vibrating resonators," in *2017 IEEE International Ultrasonics Symposium (IUS)*, 2017, pp. 1–4. doi: 10.1109/ULTSYM.2017.8092076.

[11] M. Rinaldi, C. Zuniga, and G. Piazza, "5-10 GHz AlN Contour-Mode Nanoelectromechanical Resonators," in *2009 IEEE 22nd International Conference on Micro Electro Mechanical Systems*, 2009, pp. 916–919. doi: 10.1109/MEMSYS.2009.4805533.

[12] Z. Schaffer, P. Simeoni, and G. Piazza, "33 GHz Overmoded Bulk Acoustic Resonator," *IEEE Microwave and Wireless Components Letters*, vol. 32, no. 6, pp. 656–659, 2022, doi: 10.1109/LMWC.2022.3166682.

[13] M. Kadota, T. Ogami, K. Yamamoto, H. Tochishita, and Y. Negoro, "High-frequency lamb wave device composed of MEMS structure using LiNbO_3 thin film and air gap," *IEEE Trans Ultrason Ferroelectr Freq Control*, vol. 57, no. 11, pp. 2564–2571, 2010, doi: 10.1109/TUFFC.2010.1722.

[14] M. Kadota, T. Ogami, K. Yamamoto, Y. Negoro, and H. Tochishita, "High-Frequency Lamb Wave Device Composed of LiNbO_3 Thin Film," *Jpn J Appl Phys*, vol. 48, no. 7S, p. 07GG08, Jul. 2009, doi: 10.1143/JJAP.48.07GG08.

[15] R. Lu, Y. Yang, S. Link, and S. Gong, "A1 Resonators in 128° Y-cut Lithium Niobate with Electromechanical Coupling of 46.4%," *Journal of Microelectromechanical Systems*, vol. 29, no. 3, pp. 313–319, 2020, doi: 10.1109/JMEMS.2020.2982775.

[16] J. Kramer et al., "57 GHz Acoustic Resonator with k^2 of 7.3% and Q of 56 in Thin-Film Lithium Niobate," in *International Electron Devices Meeting, San Francisco: IEEE, Dec. 2022*.

[17] R. Lu and S. Gong, "A 15.8 GHz A6 Mode Resonator with Q of 720 in Complementary Oriented Piezoelectric Lithium Niobate Thin Films," in *2021 Joint Conference of the European Frequency and Time Forum and IEEE International Frequency Control Symposium (EFTF/IFCS)*, 2021, pp. 1–4. doi: 10.1109/EFTF/IFCS52194.2021.9604327.

[18] R. Lu, Y. Yang, S. Link, and S. Gong, "Enabling Higher Order Lamb Wave Acoustic Devices With Complementary Oriented Piezoelectric Thin Films," *Journal of Microelectromechanical Systems*, vol. 29, no. 5, pp. 1332–1346, 2020, doi: 10.1109/JMEMS.2020.3007590.

- [19] W. Zhao et al., "15-GHz Epitaxial AlN FBARs on SiC Substrates," *IEEE Electron Device Letters*, vol. 44, no. 6, pp. 903–906, 2023, doi: 10.1109/LED.2023.3268863.
- [20] G. Giribaldi, L. Colombo, P. Simeoni, and M. Rinaldi, "Compact and wideband nanoacoustic pass-band filters for future 5G and 6G cellular radios." 2023. doi: <https://doi.org/10.21203/rs.3.rs-2569732/v1>.
- [21] S. Nam, W. Peng, P. Wang, D. Wang, Z. Mi, and A. Mortazawi, "An mm-Wave Trilayer AlN/ScAlN/AlN Higher Order Mode FBAR," *IEEE Microwave and Wireless Technology Letters*, pp. 1–4, 2023, doi: 10.1109/LMWT.2023.3271865.
- [22] R. Lu, Y. Yang, S. Link, and S. Gong, "A1 Resonators in 128° Y-cut Lithium Niobate with Electromechanical Coupling of 46.4%," *Journal of Microelectromechanical Systems*, vol. 29, no. 3, pp. 313–319, 2020, doi: 10.1109/JMEMS.2020.2982775.
- [23] S. Link, R. Lu, Y. Yang, A. E. Hassanien, and S. Gong, "An A1 Mode Resonator at 12 GHz using 160nm Lithium Niobate Suspended Thin Film," in 2021 IEEE International Ultrasonics Symposium (IUS), 2021, pp. 1–4. doi: 10.1109/IUS52206.2021.9593341.
- [24] Y. Shen, P. Patel, R. Vetury, and J. B. Shealy, "452 MHz Bandwidth, High Rejection 5.6 GHz UNII XBAW Coexistence Filters Using Doped AlN-on-Silicon," in 2019 IEEE International Electron Devices Meeting (IEDM), 2019, pp. 17.6.1–17.6.4. doi: 10.1109/IEDM19573.2019.8993455.
- [25] M. Hara, T. Yokoyama, T. Sakashita, M. Ueda, and Y. Satoh, "A study of the thin film bulk acoustic resonator filters in several ten GHz band," in 2009 IEEE International Ultrasonics Symposium, 2009, pp. 851–854. doi: 10.1109/ULTSYM.2009.5441576.
- [26] D. Mo, S. Dabas, S. Rassay, and R. Tabrizian, "Complementary-Switchable Dual-Mode SHF Scandium Aluminum Nitride BAW Resonator," *IEEE Trans Electron Devices*, vol. 69, no. 8, pp. 4624–4631, Aug. 2022, doi: 10.1109/ted.2022.3183963.
- [27] Y. Yang, R. Lu, L. Gao, and S. Gong, "10–60-GHz Electromechanical Resonators Using Thin-Film Lithium Niobate," *IEEE Trans Microw Theory Tech*, vol. 68, no. 12, pp. 5211–5220, 2020, doi: 10.1109/TMTT.2020.3027694.